AERODYNAMIC DESIGN OF THREE-DIMENSIONAL BIPLANE WINGS FOR LOW WAVE-DRAG SUPERSONIC FLIGHT

Daigo MARUYAMA
Dept. Aerospace Engineering, Tohoku University, Sendai 980-8579, JAPAN
Phone: +81-22-795-6981, Fax: +81-22-795-6979, Email: daigo@ad.mech.tohoku.ac.jp

Keywords: *Supersonic, Biplane, Inverse Design, CFD, Off-Design Condition*

Abstract

In supersonic flight, airfoils generate strong sonic booms and wave drags accompanied by shock waves and expansion waves. Busemann biplane is the representative airfoil which has possibility of realizing low-boom and low-drag. Aiming to realize a new concept supersonic transport, aerodynamic design and analysis are discussed based on Computational Fluid Dynamics (CFD).

Traditional biplane airfoils were extended to 3-D wings. Design Mach number is 1.7. Euler simulations were conducted. 3-D biplane wings do not have appropriate performance at areas affected by Mach cones. Tapered wings were considered to settle the issue. A tapered wing has areas which achieve better performance than 2-D biplane airfoils. Aerodynamic design of a 3-D tapered biplane wing, the taper ratio and the aspect ratio of which were 0.25 and 5.12, was conducted. A designed biplane wing accomplished lower drag than the 2-D flat-plate airfoil at C_L>0.17. Flow choking and its hysteresis which yield much amount of drag occurs at off-design conditions. A wing form from take-off to cruise state is introduced taking the issues of the drag penalty and the hysteresis into account.

1 Introduction

For the next generation of supersonic transport (SST), attaining low noise and high fuel efficiency are critical issues. The Concorde, which was the first but also the last commercial SST ever built, finished its service in 2003 due to these problems. It is necessary to develop an airplane which has low-boom and low-drag.

Busemann proposed a biplane configuration with the potential for satisfying these two conditions, by utilizing favorable interactions between the two wing elements [1,2]. The wave drag due to airfoil thickness can be nearly eliminated by a biplane configuration that promotes favorable wave interactions between the two neighboring airfoil elements (here, wave drag being defined as the resistant force on the airfoil due to the generation of shock-waves.). Licher extended the idea to reduce the wave drag due to lift [3].

In 2004, a project of supersonic transport based on those biplanes started at Tohoku University. The project has been led by Dr. Kusunose [4-6]. Fundamental analysis as well as several trials to obtain a biplane configuration has been going on [7,8].

There are many problems in realizing supersonic biplanes for a practical flight. The theories of the supersonic biplanes are based on 2-D flows. There is a possibility of not realizing optimal performance in extension to 3-D wings [9,10]. At off-design conditions, it was confirmed that the flow is choked and the choking continues to Mach numbers greater than the design Mach number in the acceleration stage. The choked flow causes very high drag compared with the cruise condition [11,12].

In this paper, the aerodynamic design of supersonic biplane wing including its off-design conditions is discussed. Beginning with the extension of 2-D supersonic biplane airfoils to 3-D wings, a 3-D biplane configuration is designed using an inverse problem approach.

Next, off-design characteristics of 3-D wings and the avoidance of choked flow are shown. Finally, a practical 3-D wing form from take-off to cruise conditions is introduced.

2 Reviews of 2-D Supersonic Biplane Airfoils

2.1 Busemann Biplane

The Busemann biplane is an airfoil which has possibility of realizing low-boom and low-drag supersonic flight. It was proposed by A. Busemann in 1935 [1,2]. As mentioned in the introduction, the wave-drag is divided into mainly two components. One is the wave-drag due to airfoil thickness (or volume), the other is that due to lift. The wave-drag due to airfoil thickness can be significantly reduced by using the concept of the Busemann biplane.

Figure 1 shows the theory of the Busemann biplane with a zero-lifted diamond airfoil. The diamond airfoil has zero-lift, but has the wave-drag due to airfoil thickness corresponding to its thickness-chord ratio. Busemann showed that the wave-drag of the diamond airfoil can be eliminated by simply splitting the diamond airfoil into two elements and locating them in a way such that the waves generated by those elements cancel each other out.

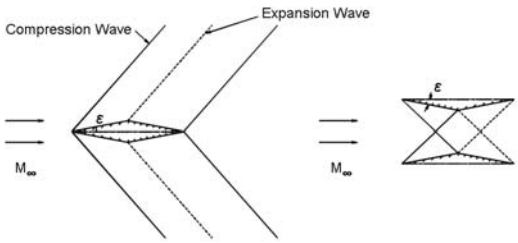

Fig. 1 Busemann Biplane

2.2 Licher Biplane

The Busemann biplane can not reduce the wave-drag due to lift although it can do that due to airfoil thickness. In 1955, Licher extended the idea of the Busemann biplane to reduce the wave-drag due to lift [3]. Generally in supersonic flight, when a biplane airfoil has no interference with waves between its two elements, it can reduce the wave-drag due to lift to half compared with a monoplane airfoil.

Figure 2 shows the theory of the Licher biplane. It is obtained by combining a lifted biplane airfoil which has partial interference of waves between its two elements (only interference of the shock wave at the leading of the upper element and the expansion wave at the mid chord of the lower element) with the Busemann biplane. As the result of it, the Licher biplane can reduce the wave-drag due to lift to two-third in addition to the reduction of that due to airfoil thickness (effects of Buseman biplane).

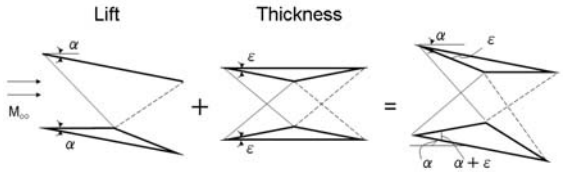

Fig. 2 Licher Biplane

2.3 Design of Biplane Airfoils

The Busemann biplane and the Licher biplane airfoils were modified to achieve higher aerodynamic performance. An inverse problem method was utilized as a design method. This method can determine an airfoil which has a specified C_p distribution. Details of the theory are described in Section **4.1**.

In this research, a flow solver named TAS code (Tohoku University Aerodynamic Simulation code) using a three-dimensional unstructured grid [13,14], was used to evaluate aerodynamic performance. In simulation, the Euler/Navier-Stokes equations are solved by a finite-volume cell-vertex scheme. The lower/upper symmetric Gauss-Seidel (LU-SGS) implicit method for an unstructured grid [15] is used for the time integration. In this research, all analyses were conducted using the Euler equations.

The Busemann biplane as baseline model, the total thickness-chord ratio of the upper and lower elements was set of 0.10 (each element is 0.05). Therefore, ε in Fig. 1 was determined to 5.71 deg. Under the condition of the free-stream Mach number 1.7, the gap between the two elements was set of 0.5. The Licher biplane airfoil has almost the same parameters as the Busemann biplane airfoil. The α in Fig. 2 was

set of 1 deg. ε was 5.71 deg. The aerodynamic performance of the Busemann biplane airfoil is C_l=0.000, C_d=0.00218 and that of the Licher biplane airfoil is C_l=0.0812, C_d=0.00449 and L/D=18.1.

The Licher biplane airfoil was modified by the inverse design method. Figure 3 shows geometries and C_p distributions of the designed biplane airfoil and the Licher biplane airfoil as an initial model. The designed biplane airfoil was termed as '2-D Designed Airfoil'. The aerodynamic performance of the '2-D Designed Airfoil' is C_l=0.115, C_d=0.00531 and L/D=21.7. The deference of C_p distributions between these two airfoils is pressure peaks at mid-chords on both elements and the C_p distributions around the trailing edge on the upper element. The latter is the most important factor in creating more lift without large increase of wave-drag.

Figure 4 shows a drag polar diagram of various 2-D airfoils. The yellow line indicates the characteristics of the 2-D zero-thickness single flat-plate airfoil. It has the lowest drag in monoplanes in this Mach number (M_∞=1.7) and has only wave-drag due to lift as drag. The '2-D Designed Airfoil' achieved lower wave-drag than the flat-plate airfoil at C_l>0.14. The details of the biplane are shown in Reference [6,7]

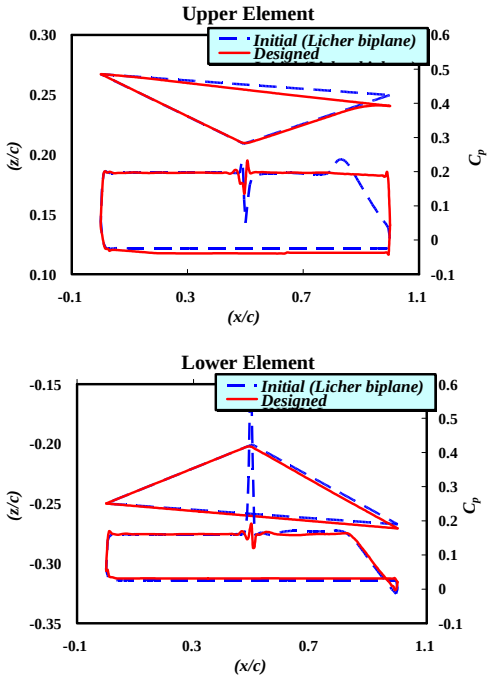

Fig. 3 Geometries and C_p Distributions of '2-D Designed Airfoil'

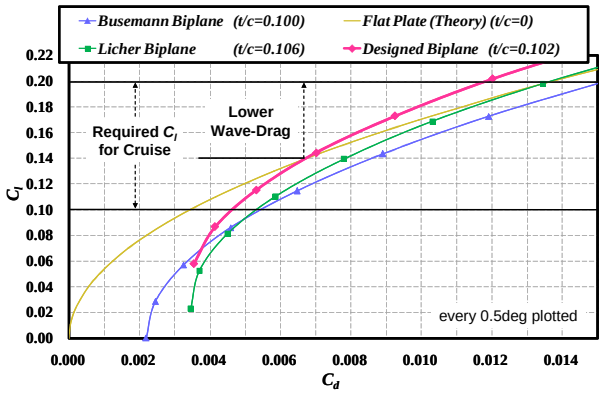

Fig. 4 Drag Polar Diagram of 2-D Airfoils

3 Aerodynamic Characteristics of 3-D Busemann Biplane Wings

3.1 Background of 3-D Busemann Biplane Wing

For a practical flight, 3-D wings should be considered. In this chapter, the drag with changes of planform of a 3-D supersonic biplane is discussed, fixing the airfoil configuration to the zero-lifted Busemann biplane airfoil. Therefore, all analyses in Chapter **3** are discussed at zero-lift conditions.

Figure 5 shows surface C_p visualization of a 3-D rectangular Busemann biplane wing. The reference area is 1. Therefore, the semi-span length is 1. The airfoil configuration is the same as the Busemann biplane airfoil shown in Section **2.3** (The total thickness-chord ratio is 0.10.). The airfoil configuration is fixed in all cases in this chapter. The number of nodes is about 1.10 million. Mach cones effects can be seen around the wing tips in Fig. 5 and they cause increase of the wave-drag. The C_D of the wing is 0.00685. It is very high compared with the C_d of the 2-D result.

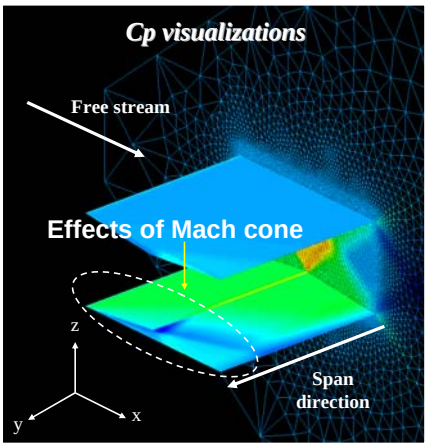

Fig. 5 Surface C_p and Mesh Visualization of Rectangular Busemann Biplane Wing (Reference Area 1)

In order to reduce the Mach cone effects around the wing tips, a tapered wing was considered. Figure 6 shows surface C_p visualization of a 3-D tapered Busemann biplane wing. The reference area and taper ratio are 1 and 0.25, respectively. Therefore, the semi-span length is 1.6. The aspect ratio is 5.12. The C_D of the wing is 0.00300. Figure 7 shows section C_d distributions of spanwise. Mach cone effects around the wing tips were significantly reduced by using the taper although the weak Mach cones were generated around the wing symmetry section. The tapered wing has another merit in section C_d. The C_ds at the areas not affected by Mach cones are lower than that of the 2-D result.

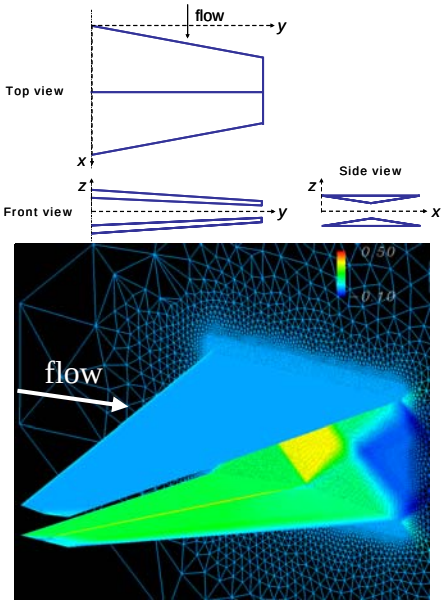

Fig. 6 Orthographic Drawing, Surface C_p and Mesh Visualization of Tapered Busemann Biplane Wing (Reference Area 1)

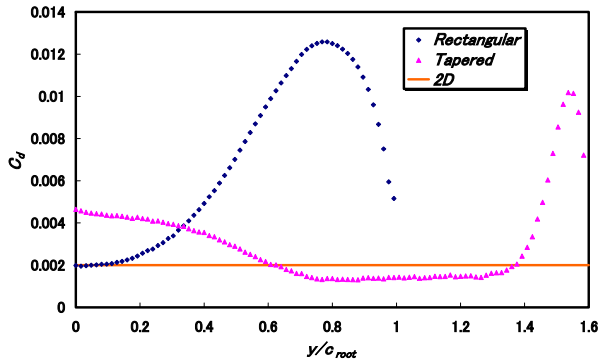

Fig. 7 Section C_d Distributions of spanwise (Zero-Lift Conditions)

3.2 Tapered Busemann Biplane Wing

3.2.1 Selection of Swept Angle

In this section, aerodynamic characteristics of various tapered wings. The airfoil configuration and the reference area are fixed in all cases in Section **3.2**. The reference area is 1. First, characteristics with changes of a swept angle of a tapered wing is discussed, fixing the taper ratio to 0.25. Figure 8 shows C_D characteristics with changes of the swept angle. The swept angle was evaluated by a coordinate of the mid chord apex at the wing tip (C_{mid}/C_{root}). The tapered wing, the C_{mid}/C_{root} of which is around 0.5 or less, achieved lowest wave-drag.

Figure 9 illustrates simple diagrams and C_d distributions of spanwise of two wings. Case1 has no sweep (C_{mid}/C_{root}=0.125). Case2 has some swept angle and its mid-chord line is vertical to the free-stream direction (C_{mid}/C_{root} =0.5). The drag reduction effect shown in Section **3.1** was not seen in Case1. Figure 10 shows C_p visualizations of the inner surfaces of Case1 and Case2, and comparison of C_p distributions of two wings at 50% semi-span stations. It can be seen that there exist the unbalance areas of the first half and the latter half about pressure levels due to 3-D effects in both cases. They determine increase and decrease of C_d of the sections not affected by Mach cones.

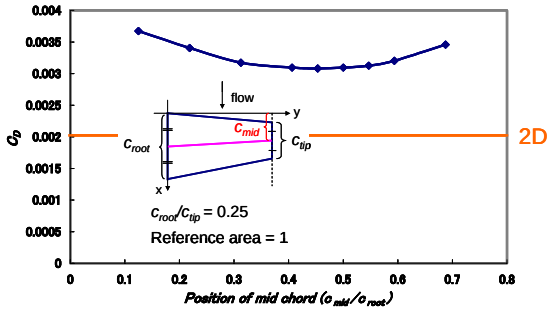

Fig. 8 C_D vs Swept Angle (Zero-Lift Conditions)

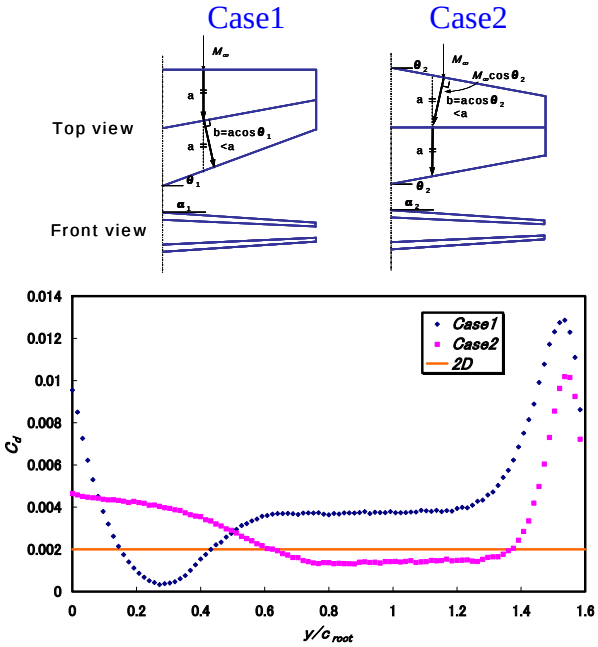

Fig. 9 Simple Diagram of Shock Waves Interaction Courses and C_d Distributions of Spanwise of Case1 and Case2 (Zero-Lift Conditions)

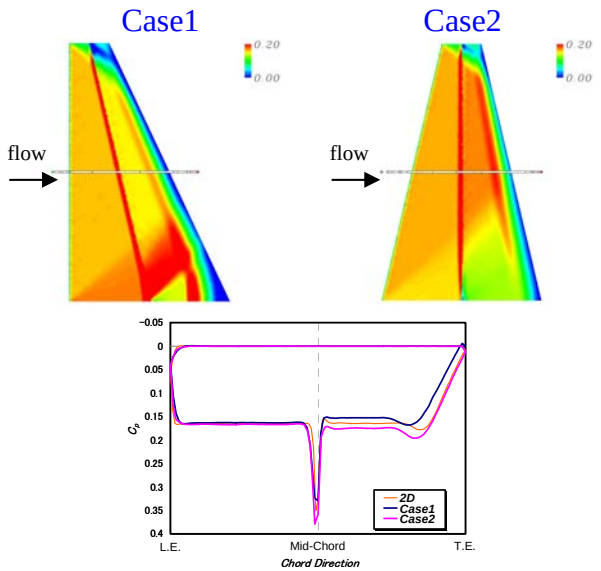

Fig. 10 C_p Visualizations of Inner Surfaces, and C_p Distributions at 50% Semi-Span Stations of Case1 and Case2

3.2.2 Selection of Taper Ratio

The characteristics of the C_D and the aspect ratio of a tapered wing were examined. The mid-chord of the wing was fixed to being vertical to the free-stream direction (C_{mid}/C_{root} =0.5 in Fig. 8). Figure 11 shows C_D and the aspect ratio characteristics with changes of the taper ratio. The smaller the taper ratio is, the lower C_D is. The aspect ratio also increases with the decrease of the taper ratio. However, C_D does not decrease with the increase of the aspect ratio at less than 0.25 of it. Therefore, a taper ratio of 0.25 was selected to avoid the increase of the aspect ratio. The aspect ratio is 5.12. In the next chapter, design of a 3-D biplane wing, the planform of which is the taper, is discussed using an inverse design approach.

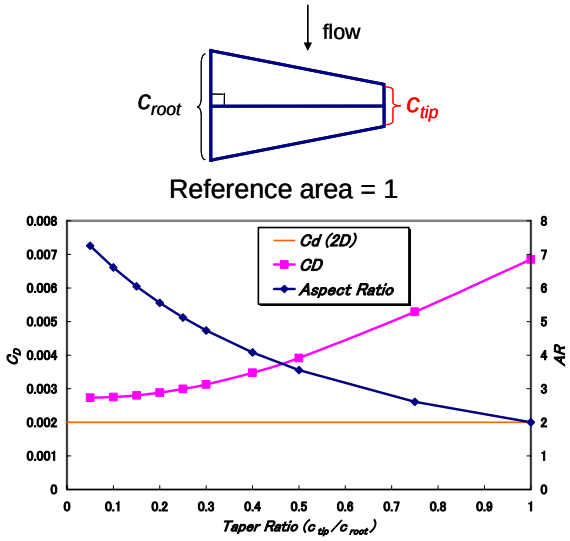

Fig. 11 C_D and Aspect Ratio Characteristics with Changes of Taper Ratio (Zero-Lift Conditions)

4 Design of 3-D Supersonic Biplane Wing

4.1 Inverse Design Method

An inverse problem approach will, in general, determine the geometry of a wing section, given a specified (target) pressure distribution. An inverse design system using the small perturbation form of the second order equation to relate pressure to local flow deflection angles has been developed.

In this design system, an airfoil's geometry *f(x)* is related to its pressure distribution by the following local oblique shock relation [2]:

$$C_p = c_1\theta + c_2\theta \qquad (1)$$

where θ and C_p represent the local flow deflection angle (df/dx-α) and pressure coefficient, respectively. Along the airfoil surface it is assumed that the local flow is tangential to the airfoil surface contour. The symbols c_1 and c_2 are the Busemann coefficients, given as

$$c_1 = \frac{2}{\sqrt{M_\infty{}^2 - 1}}, \qquad c_2 = \frac{(M_\infty{}^2 - 2)^2 + \gamma M_\infty{}^4}{2(M_\infty{}^2 - 1)^2}$$

And α is the angle of attack of the airfoil, respectively. Also, x and γ represent the airfoil-chord direction (see Fig. 12) and the ratio of specific heats.

Figure 13 illustrates the method's iterative process. First, the flow field around an initial configuration is analyzed to obtain its initial pressure distribution. Next, an inverse-problem solver is employed to calculate the x-derivative of the correction value for the airfoil geometry, $d\Delta f\pm/dx$; this x-derivative is related to the difference between the target and the current pressure distributions, denoted as ΔC_p (C_p-residual). Specifically, the geometry correction term Δf (see Fig. 12) comes from ΔC_p, using the small-perturbation forms ($C_p \rightarrow C_p + \Delta C_p$ and $f \rightarrow f + \Delta f$) of Eq. (1).

$$\Delta Cp_+ = c_1\left(\frac{d\Delta f_+(x)}{dx}\right) + 2c_2\left(\frac{d f_+(x)}{dx} - \alpha\right)\left(\frac{d\Delta f_+(x)}{dx}\right) + c_2\left(\frac{d\Delta f_+(x)}{dx}\right)^2 \qquad (2)$$

$$\Delta Cp_- = -c_1\left(\frac{d\Delta f_-(x)}{dx}\right) + 2c_2\left(\frac{d f_-(x)}{dx} - \alpha\right)\left(\frac{d\Delta f_-(x)}{dx}\right) + c_2\left(\frac{d\Delta f_-(x)}{dx}\right)^2 \qquad (3)$$

Here, + and – indicate the upper and lower surfaces, respectively. The airfoil geometry is updated by integrating the geometry correction terms:

$$f_\pm^{update}(x) = f_\pm(x) + \int_0^x \frac{d\,\Delta f_\pm}{d\,\xi}(\xi)\,d\xi \qquad (4)$$

where the symbol 0 indicates the x coordinate of the airfoil's leading edge. In this approach, however, it is obvious that there is no guarantee to obtain an airfoil that has a closed trailing edge. Therefore it may be needed that a further (but minor) modification to the specified target pressure distribution to make the trailing edge closed. Finally, the flow-field of the updated airfoil geometry is analyzed. An optimal airfoil design can be found through the repetition of this process.

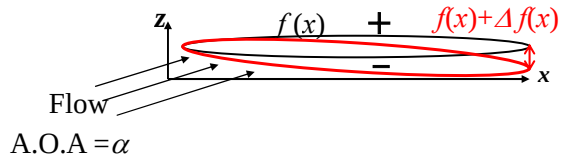

Fig. 12 Airfoil Geometries and Perturbed Geometries

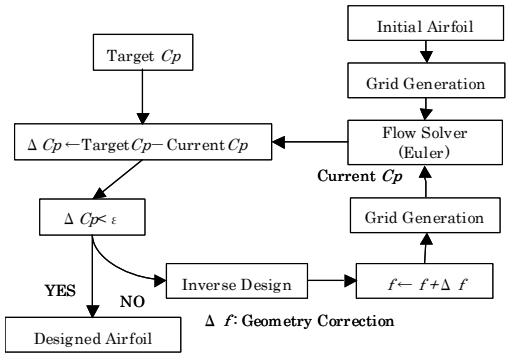

Fig. 13 Design Cycle of Inverse Problem Method

4.2 Design of Biplane Wing

4.2.1 Evaluation of Initial Model

Practical design of a 3-D supersonic biplane wing by using the inverse problem method is discussed in this section. Based on the '2-D Designed Airfoil' shown in Section **2.3** and the tapered wing as a planform determined in Sub-Section *3.2.2*, a 3-D supersonic biplane wing with higher aerodynamic performance than them is designed.

The thickness chord ratios (t/c) are about 0.10 at all span stations. The wing reference area and the taper ratio are 1 and 0.25, respectively. Therefore the semi-span length is 1.6. The aspect ratio is 5.12. Under this condition, the Busemann biplane wing with

angle of attack of 2 deg. has values of C_L=0.110, C_D=0.00706 and L/D=15.6. The 2-D airfoil configuration designed by the inverse problem method (see Fig. 3) was applied at all span stations. The biplane wing was termed '2-D Designed Wing' and has values of C_L=0.111, C_D=0.00621 and L/D=17.9. The number of nodes is about 1.10 million in all analyses in this section.

Figure 14 shows C_p visualizations of the inner surfaces and C_p distributions of the upper and lower elements of the '2-D Designed Wing'. Compared with the C_p distributions of the '2-D Designed Airfoil', large pressure peaks were confirmed on both the upper and lower elements. The values of them are very different by those of the area affected by Mach cones and those of the area not affected by Mach cones. In the upper element, the form of the C_p distribution from the pressure peak to the trailing edge is different from that of the '2-D Designed Airfoil' at each span station.

4.2.2 Design Using Inverse Problem Method

The inverse design method was applied at 10 span stations (per 10% from 0 to 90% of spanwise) at the same time. The configuration of the wing tip (100% of spanwise) was set to be the same as the initial configuration. The wing shape is defined by using the linear interpolation between each section configuration.

On the design process, some design iterations are firstly conducted on the upper element, fixing the wing configuration of the lower element (The designed wing is termed as 'Upper Designed Wing'.). Then, the lower element was designed fixing the configuration of the new designed upper element (The new designed wing is termed as 'Lower Designed Wing'). After the design process, in case the aerodynamic performance at a new designed section is worse than that of the initial, the designed section is substitute for the initial one.

Figure 15 shows target C_p distributions of the upper and lower elements and obtained C_p distributions after 14 iterations on each element. First of all, the target C_p distributions are focused on. There are two concepts in setting target C_p distributions. One is to set up the similar C_p distributions to that of the '2-D Designed Airfoil' again. The other is to creating more lift and to have higher L/D around the area affected by Mach cones (around the symmetry section) on the upper element. To put them more concretely, the first concept is for C_p distribution of each span station of the upper element to have no pressure peak and to have the similar C_p distribution of the trailing edge to that of the leading edge (see Fig. 15(a)). Concerning the lower element, only removing the pressure peak at each span station was conducted (see Fig. 15(b)). The second concept is for C_p distributions on the area affected by Mach cones (at the symmetry sections) of the upper element to be almost the same pressure levels from the mid-chords to trailing edges as those not affected by Mach cones (see Fig. 15(a)). The second concept was only applied to the upper element.

Next, the obtained C_p distributions are focused on. In each design case, design iterations were conducted on 14 times. C_p distributions of the upper element successfully converged at target ones. However, C_p distributions of the lower element did not completely converged at target ones, especially those around the wing symmetry section. Convergence at target C_p distributions were not confirmed with more iterations. It is quite likely that configurations which realize the target C_p distributions does not exist. The 'Upper Designed Wing' (the wing that only the upper element was designed in the initial model) has values of C_L=0.120, C_D=0.00662 and L/D=18.1. The 'Lower Designed Wing' (the wing that the lower element was designed after the design of the upper element) has values of C_L=0.122, C_D=0.00664 and L/D=18.3.

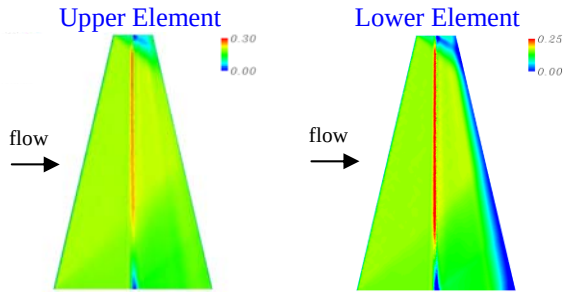

(a) Upper Element

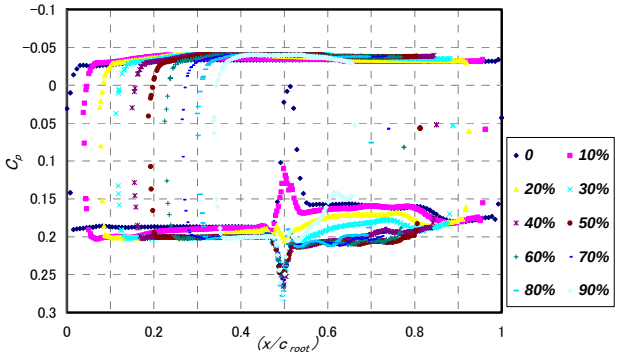

(b) Lower Element

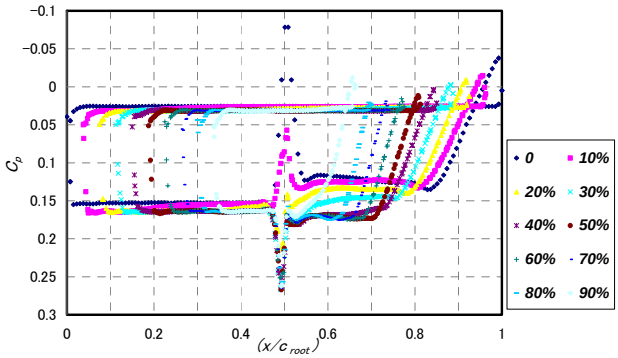

Fig. 14 Surface C_p Visualizations and C_p Distributions of Upper and Lower Elements of '2-D Designed Wing'

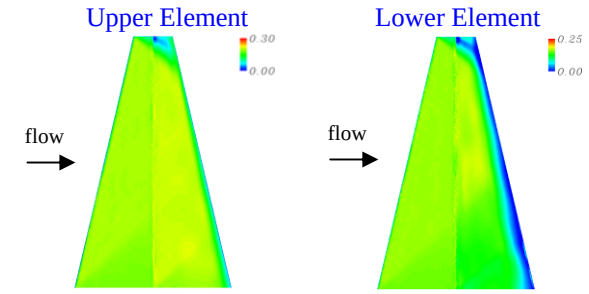

(a) Upper Element

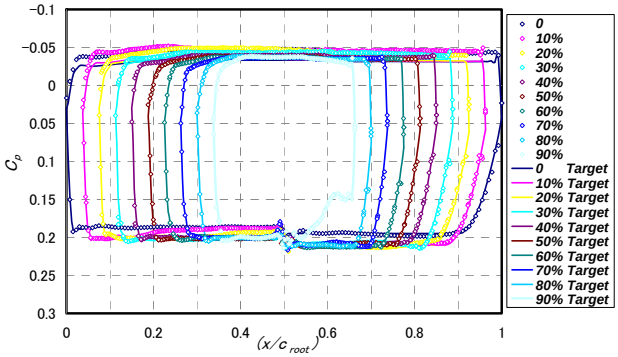

(b) Lower Element

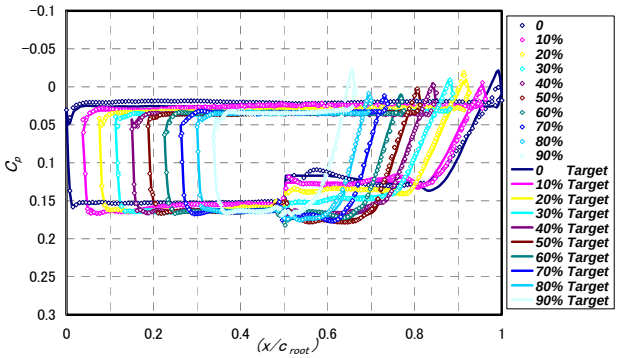

Fig. 15 Surface C_p Visualizations, Target and Obtained C_p Distributions after 14 Iterations on Each Element

(a) Upper Element

(b) Lower Element

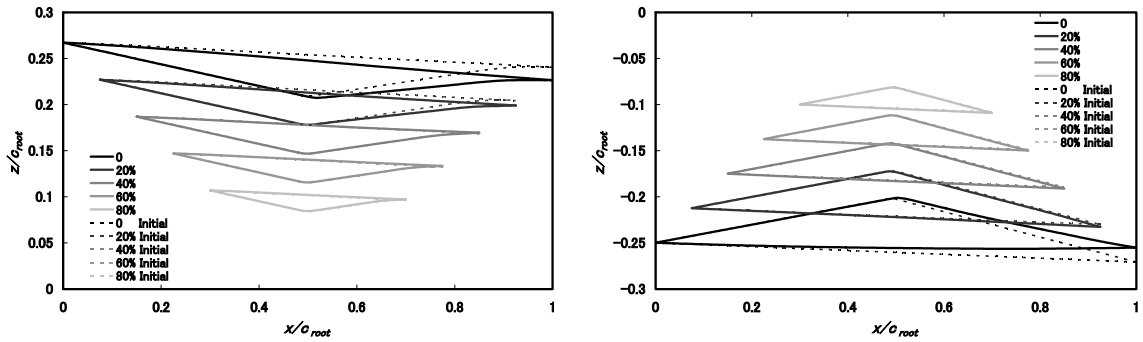

Fig. 16 Designed Geometries
(Only 5 Sections shown at Each Element)

Figures 16 and 17 show designed geometries at some span stations and section C_l, C_d and L/D distributions of spanwise of the 'Upper Designed Wing' and the 'Lower Designed Wing'.

First, the 'Upper Designed Wing' is focused on. In Fig. 16(a), the geometries around the wing symmetry section were modified to have more angles of attack. In Fig. 17, section C_ls at the areas affected by Mach cones increased without reductions of the section L/Ds.

Next, the 'Lower Designed Wing' is focused on. In Fig. 16(b), the geometry of the symmetry section was modified to have less angle of attack. In Fig. 17, section C_l and L/D got worse than those of the initial although those at the other sections were well improved.

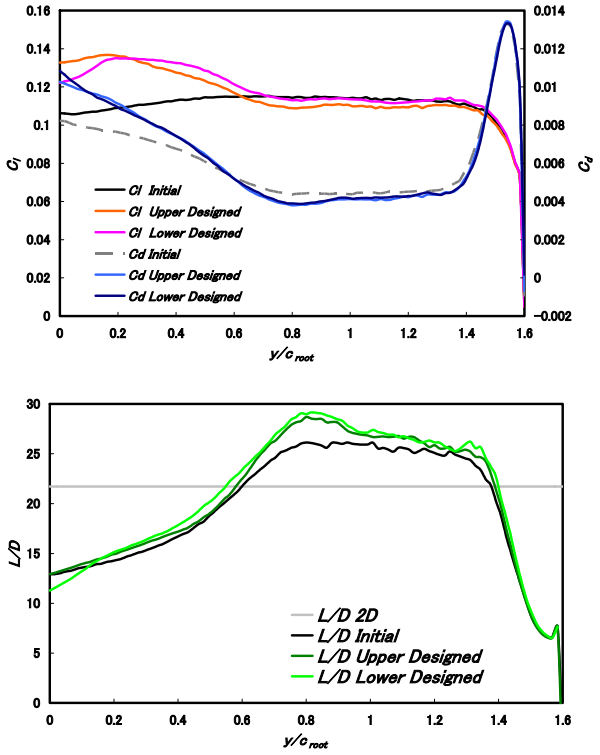

Fig. 17 Section C_l, C_d and L/D Distributions of Spanwise of 'Upper Designed Wing' and 'Lower Designed Wing'

The configuration at the symmetry section of the lower element was returned to the initial one. The wing was termed as '3-D Designed Wing'. Figure 18 shows section C_l, C_d and L/D distributions of spanwise, and C_p visualizations of the inner surfaces of the '3-D Designed Wing'. Maintaining higher L/D at all span station, more lift was created at the areas affected by Mach cones. The '3-D Designed Wing' has values of C_L=0.125, C_D=0.00678 and L/D=18.4. Table 1 shows the aerodynamic performance of the various 3-D biplane wings. The designed biplane wings have higher aerodynamic performances with lower angle of attack than the Busemann biplane wing.

Figure 19 shows a drag polar diagram of the various 3-D biplane wings including the 2-D zero-thickness single flat-plate airfoil shown in Section 2.3. The '3-D Designed Wing' has lower drag than the 2-D flat-plate airfoil at C_L >0.17.

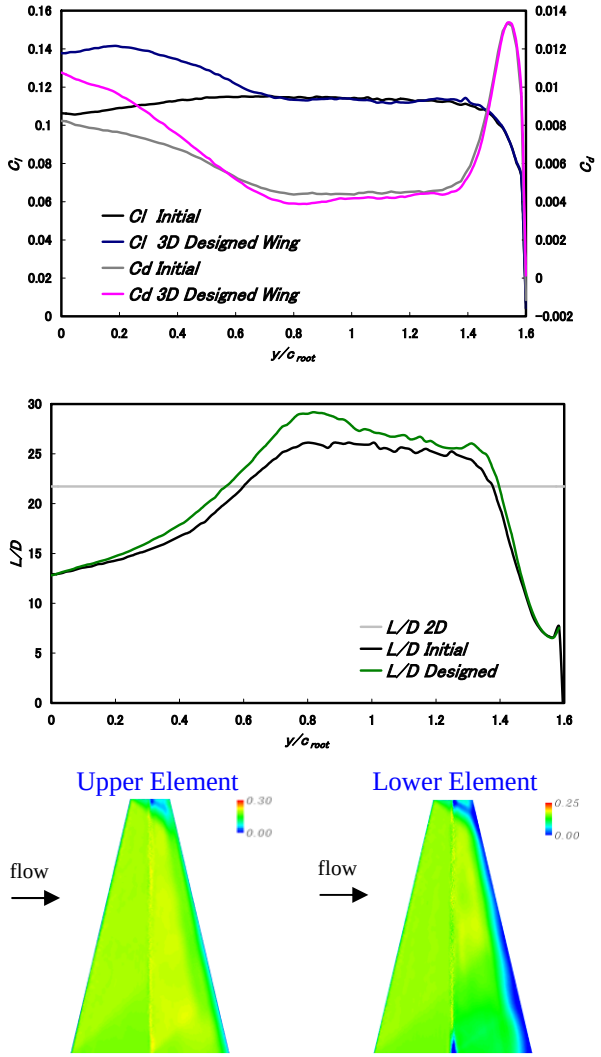

Fig. 18 Section C_l, C_d and L/D Distributions of Spanwise, and C_p Visualizations of Inner Surfaces of '3-D Designed Wing'

Table 1 Aerodynamic Performance of 3-D Wings

	C_L	C_D	L/D
Busemann biplane (α = 2deg.)	0.110	0.00706	15.6
2-D Designed Wing ($\alpha \cong$ 1deg.)	0.111	0.00621	17.9
3-D Designed Wing ($\alpha \cong$ 1deg.)	0.125	0.00678	18.4

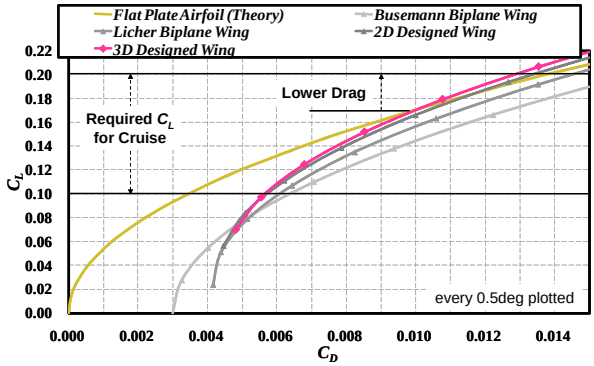

Fig. 19 Drag Polar Diagram of 3-D Wings and 2-D Zero-Thickness Single Flat-Plate Airfoil

5 Off-Design Conditions of 3-D Supersonic Biplane Wing

5.1 Tapered Busemann Biplane Wing and The Wing with Hinged Slats and Flaps

As mentioned in the introduction, supersonic biplane airfoils have very high drag at their off-design conditions [11,12]. Over a wide range more than M_∞ of 0.6, C_d increase to about 0.1 (which is about 50 times higher than that of the design point). Flow is choked at these conditions. Moreover, in acceleration stage, the choked flow continues to persist even at Mach numbers greater than the design Mach number as hysteresis. It is necessary for a supersonic transport using the biplane concept to settle these issues.

In the current study, it was confirmed that the high C_d and flow hysteresis were avoided by utilizing hinged slats and flaps which were usually used as high-lift devices (see Fig. 20) [12]. These were applied to all span stations of the 3-D tapered Busemann biplane wing.

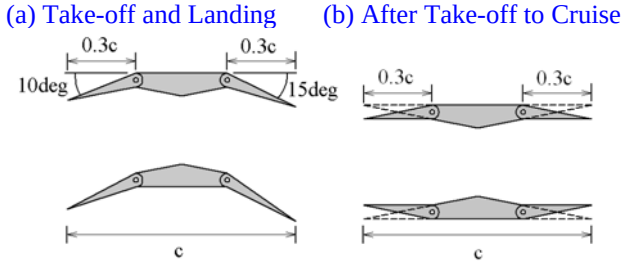

Fig. 20 Simple Diagram of Busemann Biplane Equipped with Hinged Slats and Flaps

Figure 21 shows C_D characteristics of 3-D biplane wings in the acceleration stage. The number of nodes is about 1.25 million. For comparison, characteristics of 2-D biplane airfoils and 2-D diamond airfoil which has the same thickness as the 2-D biplane airfoils are also shown in this figure. It can be seen that the drag coefficients and the critical Mach numbers (at which the choking disappeared) were reduced in both the Busemann biplane wing and that with the hinged slats and flaps compared with 2-D cases. Figures 22 and 23 show C_p visualizations of 3-D wings at M_∞=1.6 and 0.8. It can be observed that the hinged slats were useful for the reduction the critical Mach number in Fig. 22 and the hinged flaps were also useful for avoidance of acceleration to supersonic speed at the back of the throat (mid-chord) in Fig. 23.

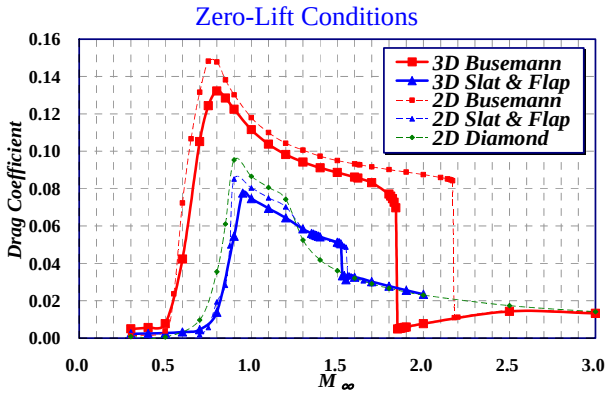

Fig. 21 Drag Coefficient Characteristics in Acceleration Stage (Zero-Lift Conditions)

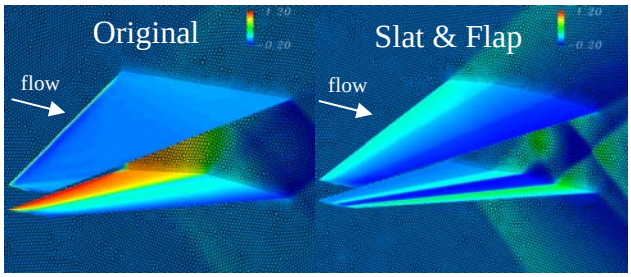

Fig. 22 Surface C_p and Mesh Visualizations at M_∞=1.6

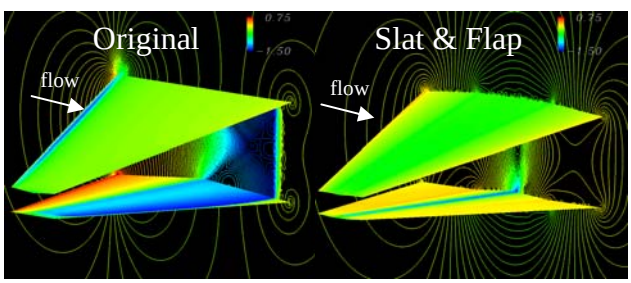

Fig. 23 Surface C_p and Contour Visualizations at M_∞=0.8

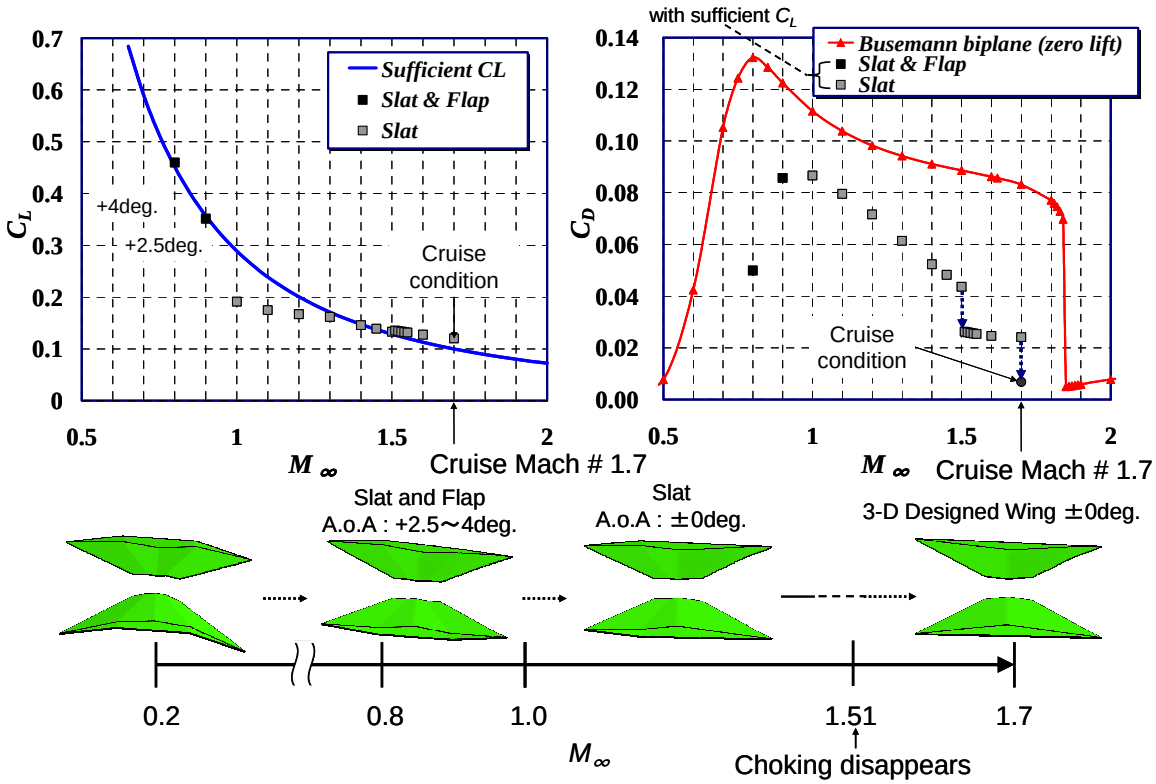

Fig. 24 Wing Form from Take-off to Cruise Conditions, C_L vs M_∞ and C_D vs M_∞

5.2 Practical Biplane Form from Take-off to Cruise Condition

In order to demonstrate an actual flight cycle of the idealized 3-D biplane wing, the concept of the hinged slats and flaps were applied to the '3-D Designed Wing'. In the present, a sufficient amount of lift was required for each flight condition. In Fig. 24, a list of biplane configurations from take-off to cruise conditions utilizing the hinged slats and flaps are illustrated. Their corresponding C_L–M_∞ and C_D–M_∞ characteristics are also given in Fig. 24.

Required aerodynamic performances at take-off and landing conditions can be assured by utilizing the hinged slats and flaps as high-lift devices. In high-subsonic flight, the hinged slats and flaps are used. This biplane wing requires some degrees of angle of attack from 2.5 to 4.0 to create a sufficient amount of lift. Then, in supersonic flight, the flaps are returned to their original positions. A biplane wing equipped with only hinged slats flies with no additional angle of attack. Thus, the biplane wing is reconfigured back to the form of the traditional biplane wing to produce good aerodynamic performance at the cruise condition, at which time hysteresis of choking disappears at M_∞=1.51.

6 Conclusions

To attain low-boom and low-drag SST, the concept of Busemann biplane was adopted. The extension of biplane airfoils to 3-D wings was attempted based on the study of 2-D biplane analysis. Design Mach number is 1.7, and total thickness-chord ratio is about 0.10. Euler simulations were conducted in this study. There are areas affected by Mach cones in 3-D biplane wings. The Mach cones produce a large amount of drag. Tapered wings were considered to reduce the effect of them. In addition, some sections not affected by Mach cones of a tapered biplane wing achieve better aerodynamic performance than 2-D biplane airfoils.

A tapered biplane wing, the taper ratio and the aspect ratio of which were 0.25 and 5.12, was selected for an inverse design approach. The designed wing has shown lower drag than the 2-D zero-thickness single flat-plate airfoil

(or the 3-D flat-plate wing with an infinite span) at C_L>0.17.

Aerodynamic performance at off-design conditions was also investigated. In the acceleration stage, it was observed that flow chocking occurred over a wide range of free-stream Mach numbers including the design Mach number (0.6<M_∞<1.84). They cause a large amount of drags. As a countermeasure of the choked flow and its hysteresis, hinged slats and flaps were utilized. The high drags were significantly reduced, as well as their range of Mach numbers. Finally, a wing form from take-off to cruise conditions was proposed. The biplane can flies with low drag and the choking disappears at M_∞=1.51.

Acknowledgements

I would like to thank Professor K. Kusunose of Ministry of Defense and Professor K. Matsushima and Professor K. Nakahashi of Tohoku University for a lot of valuable guidance and comments. The present computation was mainly performed using NEC SX-7 and NEC SX-9 of Cyberscience Center of Tohoku University. I sincerely thank all the staff for their helpful assistances.

References

[1] Busemann A. Aerodynamic lift at supersonic speeds. *Luftfahrtforschung*, Ed.12, Nr.6, pp.210-220, 1935.

[2] Liepmann H W and Roshko A. *Elements of Gas Dynamics*, John Wiley & Sons, Inc., 1957.

[3] Licher R M. Optimum Two-Dimensional Multiplanes in Supersonic Flow. *Douglass Aircraft Co.*, Report No. SM-18688, 1955.

[4] Kusunose K, Matsushima K, Goto Y, Yamashita H, Yonezawa M, Maruyama D and Nakano T. A Fundamental Study for the Development of Boomless Supersonic Transport Aircraft. *The 44th AIAA Aerospace Sciences Meeting and Exhibit*, Reno, AIAA 2006-0654, 2006.

[5] Kusunose K, Matsushima K, Goto Y, Maruyama D, Yamashita H and Yonezawa M. A Study in the Supersonic Biplane utilizing its Shock Wave Cancellation Effect. *Journal of The Japan Society for Aeronautical and Space Sciences*, Vol. 55, No. 636, pp.1-7, 2007. (in Japanese)

[6] Kusunose K, Matsushima K, Obayashi S, Furukawa T, Kuratani N, Goto Y, Maruyama D, Yamashita H and Yonezawa M. *Aerodynamic Design of Supersonic Biplane: Cutting Edge and Related Topics*. The 21st Century COE Program International COE of Flow Dynamics Lecture Series, Volume 5, Tohoku University Press, 2007.

[7] Maruyama D, Matsushima K, Kusunose K and Nakahashi K. Aerodynamic Design of Biplane Airfoils for Low Wave Drag Supersonic Flight. *The 24th Applied Aerodynamics Conference*, San Francisco, AIAA 2006-3323, 2006.

[8] Matsushima K, Kusunose K, Maruyama D and Matsuzawa T. Numerical Design and Assessment of a Biplane as Future Supersonic Transport. *Proceedings of the 25th ICAS Congress*, Hamburg, Germany, ICAS 2006-3.7.1, 1-10, 2006.

[9] Yonezawa M, Yamashita H, Obayashi S and Kusunose K. Investigation of Supersonic Wing Shape Using Busemann Biplane Airfoil. *The 45th AIAA Aerospace Sciences Meeting and Exhibit*, Reno, AIAA 2007-0686, 2007.

[10] Maruyama D, Matsushima K, Kusunose K and Nakahashi K. Aerodynamic Design of Three-dimensional Low Wave-drag Biplanes Using Inverse Problem Method. *The 46th AIAA Aerospace Sciences Meeting and Exhibit*, Reno, AIAA 2008-0289, 2008.

[11] Ferri A. Elements of Aerodynamics of Supersonic Flows. *The Macmillan Company*, 1949. (Also published as Dover Phoenix Edition, Dover Publications, Inc., New York, 2005)

[12] Maruyama D, Matsuzawa T, Kusunose K, Matsushima K and Nakahashi K. Consideration at Off-design Conditions of Supersonic Flows around Biplane Airfoils. *The 45th AIAA Aerospace Sciences Meeting and Exhibit*, Reno, AIAA 2007-0687, 2007.

[13] Nakahashi K, Ito Y, and Togashi F. Some Challenge of Realistic Flow Simulations by Unstructured Grid CFD. *International Journal for Numerical Methods in Fluids*, Vol.43, pp.769-783, 2003,

[14] Ito Y, and Nakahashi K. Surface Triangulation for Polygonal Models Based on CFD Data. *International Journal for Numerical Methods in Fluids*, Vol. 39, Issue 1, pp.75-96, 2002.

[15] Sharov D and Nakahashi K. Reordering of Hybrid Unstructured Grids for Lower-Upper Symmetric Gauss-Seidel Computations. *AIAA Journal*, Vol.36, No.3, pp.484-486, 1998.

Copyright Statement